BMC Genomics

RESEARCH

Open Access

# M6A methyltransferase METTL3 promotes glucose metabolism hub gene expression and induces metabolic dysfunction-associated steatotic liver disease (MASLD)

Shuowen Wang[1,2,5], Ziying Xu[3], Zijun Wang[4], Xiaoyu Yi[5] and Jianxin Wu[2,5,6*]

## Abstract

**Background** N6-methyladenosine (m6A) RNA modification plays a crucial role in various biological events and is implicated in various metabolic-related diseases. However, its role in MASLD remains unclear. This study aims to investigate the impact of METTL3 on MASLD through multi-omics analysis, with a focus on exploring its potential mechanisms of action.

**Methods** An MASLD mouse model was established by feeding C57BL/6J mice a high-fat diet for 12 weeks. A METTL3 stable overexpression AML12 cell model was also constructed via lentiviral transfection. Subsequent transcriptomic and proteomic analyses, as well as integrated analysis between different omics datasets, were conducted.

**Results** METTL3 expression was significantly increased in the MASLD mouse model. Through our transcriptomic and proteomic analyses, we identified 848 genes with significant inconsistencies between the transcriptomic and proteomic datasets. GO/ KEGG enrichment analyses identified terms that may be involved in post-transcriptional modifications, particularly METTL3-mediated m6A modification. Subsequently, through integrated proteomic analysis of the METTL3-overexpressed AML12 cell model and the MASLD mouse model, we selected the top 20 co-upregulated and co-downregulated GO/ KEGG terms as the main biological processes influenced by METTL3 during MASLD. By intersecting with pathways obtained from previous integrated analyses, we identified GO/ KEGG terms affected by METTL3-induced m6A modification. Protein-protein interaction analysis of proteins involved in these pathways highlighted GAPDH and TPI1 as two key hub genes.

**Conclusions** During MASLD, METTL3 regulates the glycolytic pathway through m6A modification, influencing the occurrence and development of the disease via the key hub genes GAPDH and TPI1. These findings expand our understanding of MASLD and provide strong evidence for potential therapeutic targets and drug development.

**Keywords** MASLD, m6A, Proteomic, METTL3, Transcriptome

*Correspondence:
Jianxin Wu
jianxinwu_tongren@163.com
[1]Gastroenterology Department, Children's Hospital Capital Institute of Pediatrics, Beijing 100020, China
[2]Beijing Municipal Key Laboratory of Child Development and Nutriomics, Capital Institute of Pediatrics, Beijing 100020, China
[3]Bacteriology Department, Capital Institute of Pediatrics, Beijing 100020, China
[4]Beijing Shijitan Hospital, Capital Medical University, Beijing 100038, China
[5]Department of Biochemistry and Immunology, Capital Institute of Pediatrics, Beijing 100020, China
[6]Beijing Tongren Hospital, Capital Medical University, Beijing 100005, China

## Introduction

The concept of nonalcoholic fatty liver disease (NAFLD) was first proposed in the 1980s, but with a deeper understanding of the condition [1], there arose an urgent need for a more neutral and accurate term to name the disease. Therefore, in 2023, supported by over 200 liver disease experts from multiple international liver disease research associations, there was a proposal to rename NAFLD as metabolic dysfunction-associated steatotic liver disease (MASLD). This change aims to reduce the stigma associated with the disease, enhance awareness and understanding, and drive the development of drugs/biomarkers [2]. A retrospective study found that 98% of individuals meeting the criteria for NAFLD also met the criteria for MASLD [3].

MASLD is an umbrella term encompassing a continuum of liver conditions, extending from metabolic dysfunction-associated steatotic liver (MASL) to metabolic dysfunction-associated steatohepatitis (MASH) [4]. MASL is defined by an accumulation of triglycerides within liver cells, accompanied by minimal or absent inflammation and the absence of hepatocyte ballooning, and it is often reversible. To fall within the MASLD spectrum, steatosis must be linked to at least one cardiometabolic risk factor such as obesity [5], dyslipidemia, hypertension, or insulin resistance, excluding excessive alcohol consumption [2].

Epidemiological studies using MASLD diagnostic classifications have found that 20–30% of adults with MASL progress to MASH [6], with approximately 20–50% of MASH patients nearing the progression to cirrhosis [7]. In the pediatric population diagnosed with MASLD through biopsy, 25–50% have MASH, and 10–25% initially present with advanced fibrosis [8–12]. Even in patients who do not progress to cirrhosis, approximately 13–49% of hepatocellular carcinoma (HCC) cases occur in individuals with non-cirrhotic MASH [13]. It is estimated that by 2030, over 300 million individuals in China, over 100 million in the United States, and 15 to 20 million in major European countries will have MASLD [14].

An increasing body of research has demonstrated the significant role of m6A in the occurrence and development of MASLD [15]. A recent study on MASLD patients found differential m6A modifications in 176 mRNA and 44 lncRNA between healthy and MASLD liver tissues, with differential modifications primarily enriched in biological processes related to transcriptional regulation and carboxylic acid metabolism [16]. In a mouse model of MASLD induced by a high-fructose diet, researchers identified 266 differentially expressed genes (DEGs) altering m6 modification levels using RNA transcriptome sequencing and m6A RNA immunoprecipitation sequencing, indicating that the majority of highly methylated genes are associated with lipid metabolism [17]. Similar results were observed in mice with fatty liver induced by a high-fat diet (HFD) [18]. Cheng and colleagues found, through bioinformatics methods, that in comparison to the control group, m6A regulatory factors METTL3/14 and FTO were elevated in MASLD patients, while WTAP, RBM15, YTHDC1, YTHDC2, IGF2BP1, HNRNPC, and HNRNPA2B1 were decreased [19].

The m6A "writers," that is m6A methyltransferases, form a multi-component methyltransferase complex that catalyzes m6A modification, collectively regulating the transfer of methyl groups from S-adenosyl methionine to the adenine base of RNA [20]. These enzymes include methyltransferase-like 3 (METTL3), METTL5, METTL14, METTL16, Wilms tumor 1-associated protein (WTAP), Vir-like m6A methyltransferase associated (also known as KIAA1429), RNA-binding motif protein 15/15B (RBM15/15B), zinc finger CCCH-type containing 13 (ZC3H13), and HAKAI (also known as CBLL1, a ring finger-type E3 ubiquitin ligase) [21–24]. Of these m6A methyltransferases, METTL3 and METTL14 exert the most significant impact on m6A RNA methylation. The core subunit of the m6A-METTL complex, METTL3, contains a unique methyltransferase catalytic domain, and it interacts with METTL14 to form the active m6A-METTL complex, termed METTL3/ METTL14 heterodimer. In the heteromeric m6A-METTL complex, METTL14 binding to METTL3 is known to provide functional support [22, 25].

METTL3 overexpression has been reported to enhance the expression of Rubicon mRNA, inhibiting autophagosome-lysosome fusion, hindering autophagic degradation, and thus reducing hepatic lipid clearance during MASLD [26]. However, Qin et al. [27] found that loss of METTL3 in myeloid cells slows down the progression of MASLD by reducing m6A modification of DNA damage-inducible transcript 4 (DDIT4), which plays a crucial role in regulating macrophage activation by lowering mTOR and NF-κB signaling pathway activity. By increasing the expression level of DDIT4, they concluded that METTL3 plays an important role in accelerating MASLD development by increasing m6A modification of DDIT4. Additionally, Xie et al. [28] confirmed that elevated METTL3 promotes liver insulin resistance (IR) and stimulates lipid synthesis by n6-methylation of fatty acid synthase mRNA, thereby increasing its overall mRNA levels. Zhong et al. [29] found that knocking out YTHDF2 or METTL3 in vitro could increase the stability of peroxisome proliferator-activated receptor (PPAR) α mRNA and the expression of PPARα, thereby reducing lipid accumulation. Li et al. [30] found that the levels of m6A and the expression of METTL3 increased in the livers of mice fed with HFD. Overall, these studies collectively support the role of METTL3 in promoting MASLD.

Although MASLD imposes a significant burden clinically, there are currently no approved drug therapies for the prevention or treatment of MASLD, despite ongoing exploration of numerous potential pathways [31, 32]. Understanding the mechanisms underlying MASLD is crucial for the development of new therapeutic targets and prognostic markers. However, research on the relationship between METTL3-mediated m6A post-transcriptional modification and MASLD is limited. By exploiting recent advances in "omics" technologies that have made large-scale molecular analysis of biological systems possible, we report here an investigation of the relationship between METTL3 and MASLD in a mouse model through multi-omics analysis.

In the MASLD animal model, a multi-omics integrated analysis was conducted on the transcriptome and proteome to identify pathways exhibiting differential expression and inconsistent trends between the two datasets, indicative of potential pathways under epigenetic regulation. Given the overexpression of METTL3 in MASLD, we established an AML12 cell line overexpressing METTL3 for proteomic analysis. Enriched pathways regulated by METTL3 were identified, and further intersection analysis was performed between these pathways and the proteomic pathways in the MASLD model to pinpoint pathways potentially regulated by METTL3 in MASLD. Subsequent intersection of these pathways with those potentially under epigenetic regulation revealed pathways in MASLD potentially modulated by METTL3-mediated m6A regulation (Fig. 1). This research should provide a foundation and a direction for future research on the impact of m6A methyltransferase METTL3 on MASLD.

## Materials and methods

### MASLD mouse model establishment

In line with previous modeling methods, this study utilized adult male C57BL/6J mice (Charles River Laboratory), aged 8 weeks and weighing 20–22 g [33]. After a one-week acclimation period, the mice were divided into two groups: one group was fed a high-fat diet (HFD, Product D12492, sourced from Research Diets) for 12 weeks to establish the MASLD model, while the other group received a standard chow diet as the control group. The entire animal study protocol was thoroughly reviewed and subsequently received ethical approval

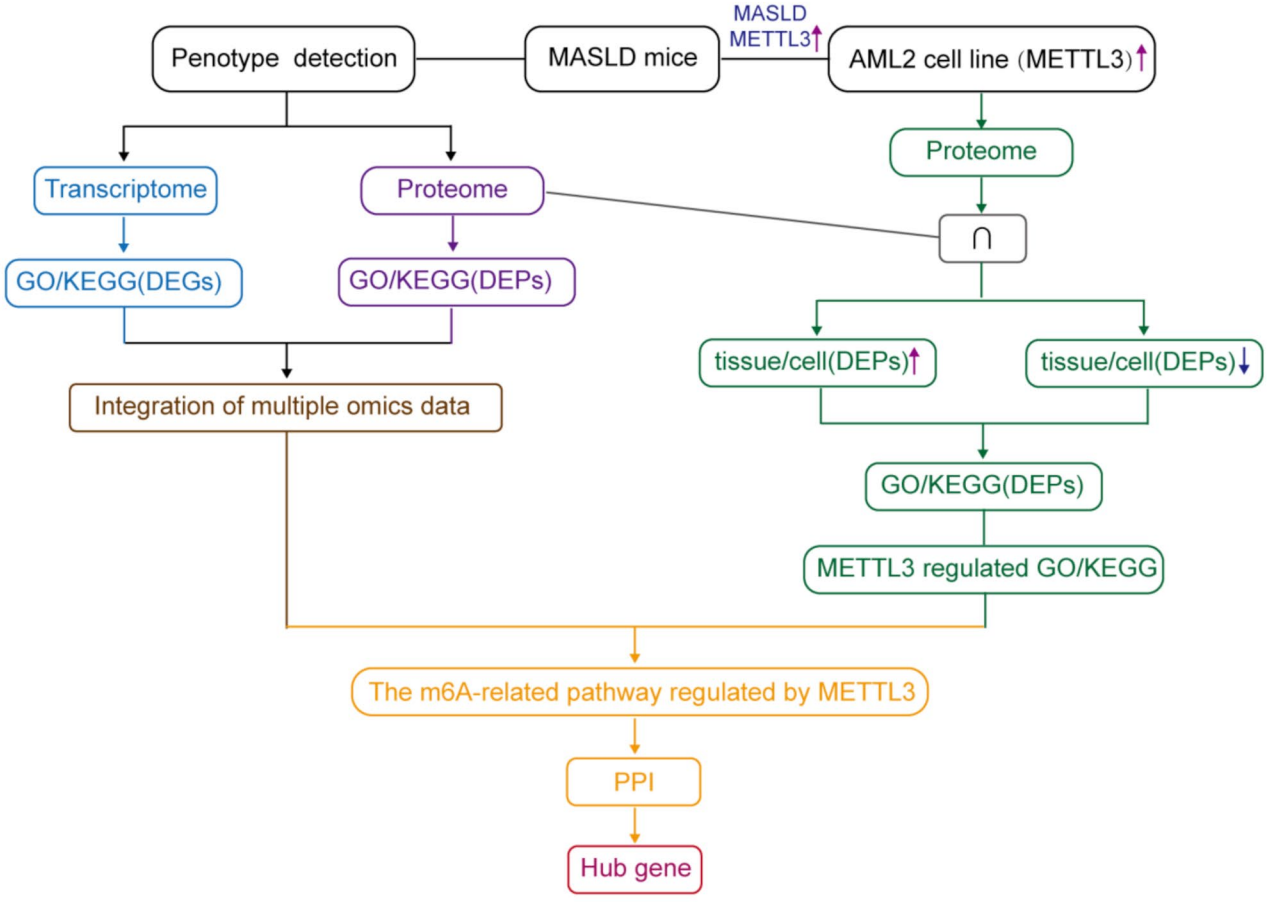


**Fig. 1** Technology roadmap: contains the overall design thinking for this study

from the Animal Care and Protection Committee of the Capital Institute of Pediatrics (Approval number, SHERLL2021032). After 12 weeks, the mice were euthanized with $CO_2$, and their livers were perfused with saline until whitish. The liver tissues were carefully excised, frozen in liquid nitrogen, and stored at -80℃ for analysis, preserving sample integrity.

#### Hematoxylin and Eosin (H&E) staining

Mouse liver tissues preserved in paraffin were sectioned into 5 μm slices and then subjected to H&E, Masson, and Sirius red staining. Fresh liver tissues were embedded in Tissue-Tek OCT compound and cut into 10 μm sections for oil red O staining to detect lipid droplets. All the samples were examined at 200× magnification via a Nikon ECLIPSE 50i microscope (Nikon, Tokyo, Japan).

#### Immunohistochemistry (IHC)

Mouse liver tissues preserved in paraffin were sectioned into 5 μm slices and subjected to immunohistochemistry (IHC). After deparaffinization and rehydration, antigen retrieval was performed by heating the sections in citrate buffer (pH 6.0) in a pressure cooker. Endogenous peroxidase activity was blocked using a 3% hydrogen peroxide solution. The tissue sections were incubated overnight at 4 °C with primary antibodies specific to target proteins, followed by incubation with HRP-conjugated secondary antibodies. The antigen-antibody complexes were visualized using a DAB substrate kit, and the sections were counterstained with hematoxylin. All stained samples were examined at 200× magnification using a Nikon ECLIPSE 50i microscope (Nikon, Tokyo, Japan) to evaluate protein expression patterns in liver tissue.

#### Cell culture and transfection

AML12 cell lines were sourced from BeNa Culture Collection and cultured in DMEM (Life Technology) with 10% fetal bovine serum, 1% penicillin/streptomycin, ITS solution (Life Technology), and 40 ng/mL dexamethasone at 37 °C in 5% CO2. Synthetic METTL3-coding sequences were inserted into a cloning vector and co-introduced with psPAX2 and pMD2G into HEK293T cells for lentivirus production, as described previously [33]. The lentivirus was used to infect AML12 cells for 24 h, followed by selection with 2 μg/mL puromycin for 6 days.

#### Western blot

Western blot was done as described previously [33]. To determine the protein levels of METTL3, we used a specific antibody from Cell Signaling Technology (catalog number 86132). The expression of GAPDH, ENO1, TPI1, and β-Actin was assessed using antibodies from ABclonal (catalog numbers A19056, A1033, A2579, and AC026, respectively). Additionally, H3 protein levels were measured with an ABclonal antibody (catalog number A2348), ensuring a comprehensive evaluation of protein expression in our experiments.

#### Quantitative real-time PCR (qRT-PCR)

Quantitative real-time PCR (qRT-PCR) was done as described previously [34]. Gene expression analysis was meticulously conducted applying the relative quantification $2^{-\Delta\Delta Ct}$ method, with 18 S rRNA serving as the endogenous reference for normalization. Mouse GAPDH qPCR Primer Pair (Forward Primer-AGGTCGGTGTGA ACGGATTTG; Reverse Primer- TGTAGACCATGTAG TTGAGGTCA), Mouse ENO1 qPCR Primer Pair (Forward Primer- TGCGTCCACTGGCATCTAC; Reverse Primer- CAGAGCAGGCGCAATAGTTTTA), Mouse TPI1 qPCR Primer Pair (Forward Primer- CCAGGAAG TTCTTCGTTGGGG; Reverse Primer- CAAAGTCGAT GTAAGCGGTGG).

#### Liquid chromatography-tandem mass spectrometry analysis

Samples were retrieved from − 80 °C storage and immediately lysed by ultrasonication in a buffer containing 8 M urea and 1% protease inhibitor cocktail. After centrifugation at 12,000 g for 10 min at 4 ℃, the supernatants were transferred to new tubes for protein concentration determination using the BCA Protein Assay Kit. Liquid chromatography-tandem mass spectrometry of the samples was performed at PTM Bio lab (Hangzhou, China). The liquid chromatography-tandem mass spectrometry procedure was performed as previously described [33, 35, 36]. Briefly, we employed the 4D label-free quantification (LFQ) technique to analyze protein digested peptides via liquid chromatography-tandem mass spectrometry (LC-MS/MS). Peptides were first separated using the EASY-nLC 1200 ultra-high-performance liquid chromatography (UHPLC) system, then introduced into the NSI ion source for ionization, before being analyzed using the Orbitrap Exploris 480 mass spectrometer. The resulting MS/MS data were processed using the Proteome Discoverer search engine (v.2.4). Tandem mass spectra were searched against the Musmusculus10090SP20230103. fasta database (17132 entries), concatenated with a reverse decoy and contaminants database. The proteomics data has been uploaded to the public database ProteomeXchange.

(https://proteomecentral.proteomexchange.org/cgi/GetDataset? ID=PXD047819; https://proteomecentral.proteomexchange.org/cgi/GetDataset? ID=PXD050565)

#### Transcriptomics sequencing

Total RNAs were extracted from liver tissue samples using TRIzol reagent. All sequencing was performed on

the DNBseq platform using the PE150 strategy. Clean reads were derived from the RNA-sequencing data by eliminating sequences with low quality, including adapter sequences, sequences with a quality score > 10% in raw reads, and sequences shorter than 25 base pairs. The clean reads were then aligned to the reference genome GCF000001635.27GRCm39 using HISAT. The raw data of the transcriptomics has been deposited into the SRA public dataset.

(https://www.ncbi.nlm.nih.gov/bioproject/PRJNA1052390)

#### Transcriptome and proteomics analyses

A differential expression analysis was performed using DESeq, yielding $\log_2$ fold-change ($\text{Log}_2$FC) and q-values for each comparison group. To minimize false positives, *p*-values were adjusted with the Benjamini-Hochberg correction (q-value). Transcripts with $\text{Log}_2\text{FC} > 1$ and q-value < 0.05 were classified as significantly upregulated, while those with $\text{Log}_2\text{FC} < -1$ and q-value < 0.05 were downregulated. For proteomic quantification, relative expression ratios and *p*-values were analyzed, with no further FDR correction required due to smaller data volume. Proteins with a ratio < 1.2 and *p*-value < 0.05 were considered significantly upregulated, and those with a ratio > 1.2 and *p*-value < 0.05 were downregulated.

#### GO and KEGG

After identifying significantly differentially expressed transcripts and proteins in each comparison group (using the aforementioned criteria), we conducted Gene Ontology (GO) and Kyoto Encyclopedia of Genes and Genomes (KEGG) enrichment analyses. For proteomic data, a *p*-value threshold of < 0.05 was used, and for transcriptomic data, a q-value threshold of < 0.05 was applied. GO term enrichment analysis was carried out using the Eggnog-mapper software (version 5.0.2, http://eggnog5.embl.de/#/app/home) based on the EggNOG database. The GO annotation process involved using Eggnog-mapper to extract GO IDs from the identified proteins according to the EggNOG database and performing functional classification annotation based on cellular components, molecular functions, and biological processes. Each gene or protein was associated with terms from the GO database, which includes three major categories: Molecular Function (MF), Biological Process (BP), and Cellular Component (CC).

For KEGG annotation, we employed Diamond software (version 2.0.11.149) to perform gene or protein annotation based on the KAAS (KEGG Automatic Annotation Server, April 3, 2015, http://www.genome.jp/kegg/kaas/) database. This allowed us to associate genes or proteins with metabolic pathways, signaling pathways, and biological functional modules within the KEGG database. Functional annotation was provided by linking the proteins to KEGG IDs. Protein pathway annotation was performed by comparing sequences through BLAST (blastp, e-value ≤ 1e-4), where the top-scoring result was used for each sequence.

#### Statistical analyses

All reported data were obtained from at least three independent experiments. The data were then analyzed using GraphPad Prism software (version 8; GraphPad, La Jolla, CA, USA). The results are presented as mean ± standard deviation (SD). Group comparisons were conducted using a two-tailed unpaired Students t-test. Differences yielding a *p*-value < 0.05 were deemed statistically significant ($^{*}p < 0.05$, $^{**}p < 0.01$, $^{***}p < 0.001$, $^{****}p < 0.0001$).

## Results

#### METTL3 expression is significantly increased in MASLD

We established a mouse model of MASLD through 12 weeks of HFD, and we subsequently performed transcriptomic sequencing and proteomic profiling of the mouse liver (Fig. 2A). Observation of H&E stained liver tissue sections revealed diffuse macro-vesicular changes in hepatocytes after HFD feeding, likely due to lipid droplet accumulation. Oil Red O staining and Sirius Red staining further confirmed the pathological state of the mouse liver, which was characterized by lipid droplet accumulation without evident fibrosis (Fig. 2B and C). Consistent with most literature findings, we also observed a significant increase in METTL3 expression in the MASLD mouse model (*p*-value = 0.0008) (Fig. 2D and E). In particular, the immunohistochemistry results revealed an elevated expression of METTL3 in the nucleus (Fig. 2E).

#### MASLD has a significant impact on the transcriptomic profile of mouse liver tissue

Through transcriptome sequencing analysis, we aimed to identify the transcriptomic changes in the liver tissue of mice with MASLD. To ensure the accuracy and reliability of the obtained data, rigorous quality control measures were applied to the transcriptome sequencing data (Figure S1). We performed RNA analysis using the Agilent 2100, and the results indicated that the RNA 28 S/18S ratio was greater than 1.5, and the RNA Integrity Number (RIN) was greater than 7, demonstrating good quality and integrity of the RNA suitable for library construction (Figure S1A-S1C). Subsequently, we employed Pearson correlation coefficients and Principal Component Analysis (PCA) to demonstrate the correlation and characteristics of gene expression among samples. The results showed high intra-group correlation, inter-group differences, and no sample outliers (Figure S1D-S1E). Following this, box plots, density plots, and bar graphs were utilized to illustrate the good distribution of sequencing

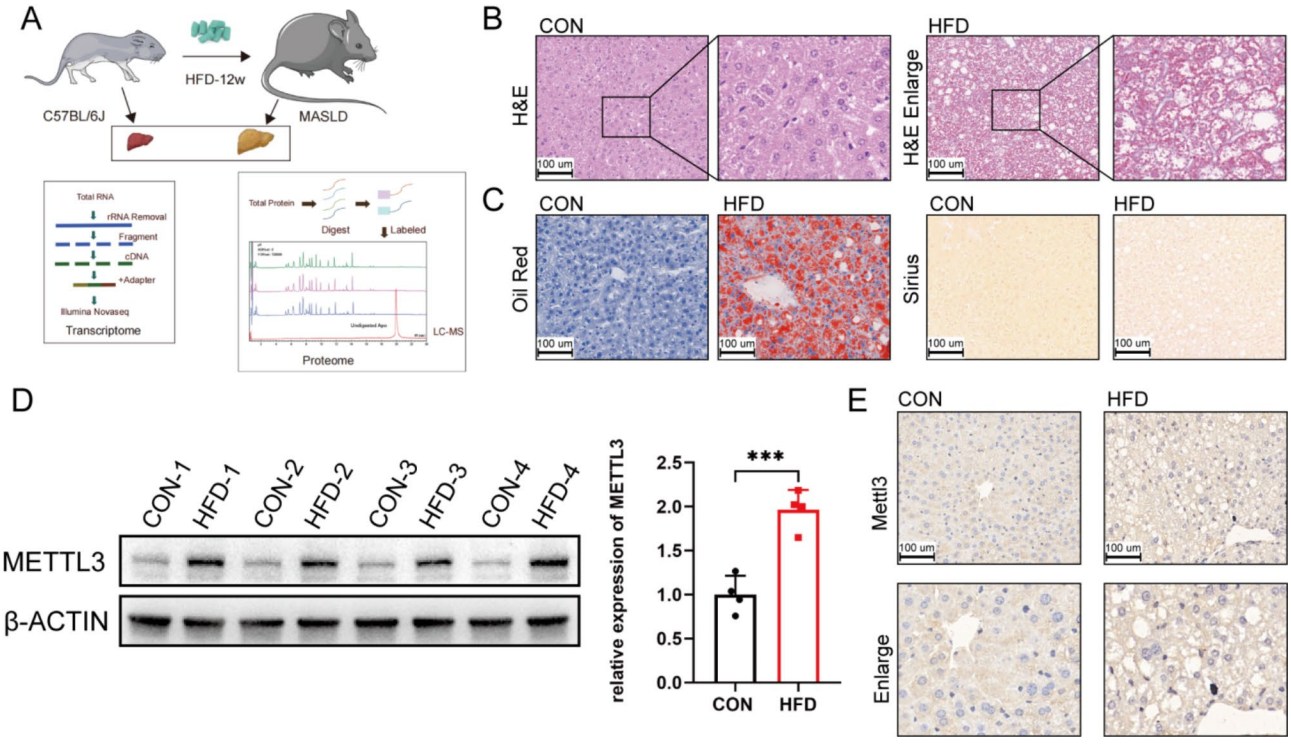


**Fig. 2** Significant Increase of METTL3 in MASLD. (**A**) Schematic representation of the modeling process. Male wild-type mice were subjected to high-fat diet feeding for 12 weeks, followed by transcriptomic and proteomic analysis. (**B**) Liver sections stained with H&E. Scale bar, 100 μm. (**C**) Liver sections stained with Oil Red and Sirius Red. Scale bar, 100 μm. (**D**) Western blotting and quantitative analysis of METTL3 protein in the MASLD mouse model. (**E**) Immunohistochemistry staining of METTL3 in liver sections of the MASLD mouse model. Scale bar, 100 μm. ($n = 4$, t-test, $^{*}p < 0.05$, $^{**}p < 0.01$, $^{***}p < 0.001$, $^{****}p < 0.0001$)

data (Figure S1F-S1H). Subsequently, using $|\log_2 FC| > 1$ and q-value < 0.05 as the threshold criteria, we compared gene expression between the control (CON) group and the HFD group, identifying a total of 386 differentially expressed genes (DEGs), 211 upregulated genes and 175 downregulated genes (Fig. 3A and B).

Gene Ontology (GO) and Kyoto Encyclopedia of Genes and Genomes (KEGG) enrichment analyses are common bioinformatics methods used to understand the functions and regulatory mechanisms of DEGs in different biological processes. Using these enrichment analyses, we identified and displayed here the enriched pathways based on the top 20 terms with the smallest q-values (Fig. 3C and F). In the GO enrichment analysis at the BP level, we found that the terms were mainly concentrated in metabolic processes, and (to a lesser extent) biological responses, and biological rhythms. Within metabolic processes, the DEGs were especially enriched in the processes of lipid metabolism and organic acid metabolism (Fig. 3C). At the CC level, the enriched terms included various cellular and molecular components that are crucial for understanding cell structure and function, including cell membranes, organelles, protein complexes, and extracellular structures (Fig. 3D). At the MF level, terms related to oxidoreductase activity, protein binding, and enzyme activity were especially enriched (Fig. 3E). These three levels of enrichment analysis in GO enrichment constitute the core structure, providing a hierarchical way to understand the functions of DEGs. The enriched pathways in KEGG analysis included vitamin metabolism, fatty acid metabolism, hormone biosynthesis, biosynthesis and metabolism pathways, signaling pathways, and sugar metabolism. Further investigation into these pathways should contribute to understanding the complex biological regulatory networks and the mechanisms underlying the occurrence of MASLD (Fig. 3F).

### MASLD has a significant impact on the proteomic profile of mouse liver tissue

Due to the regulatory effects of post-transcriptional and post-translational modifications, mRNA expression levels may not accurately reflect protein levels. Therefore, we conducted a proteomic analysis to examine the impact of MASLD at the level of proteins, the primary executors of cellular functions. During the process of protein mass spectrometry analysis, rigorous quality control measures were implemented to ensure the accuracy of our results (Figure S2). We evaluated the protein quality using Coomassie brilliant blue staining. The results revealed clear and distinct protein bands in all lanes,

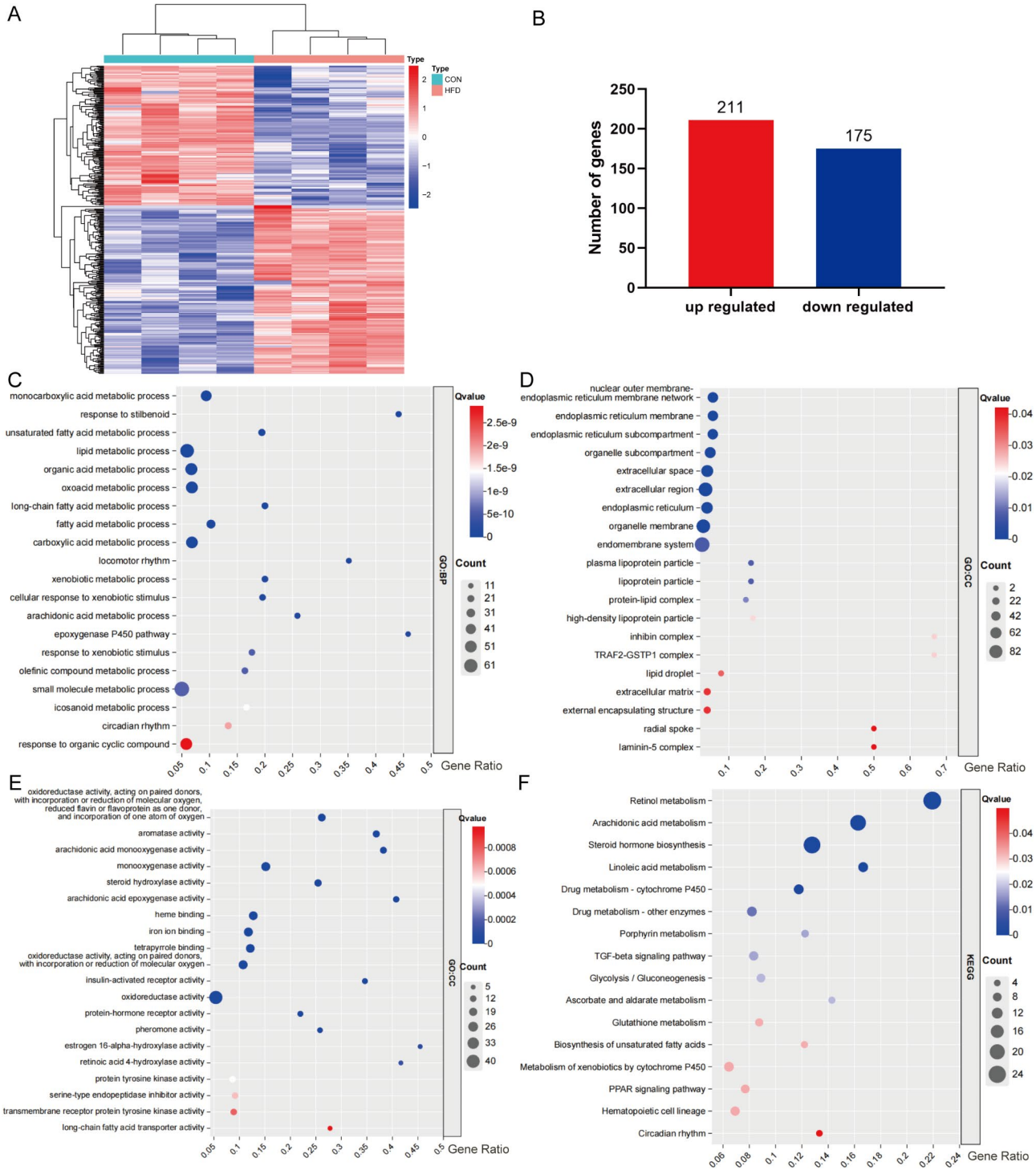


**Fig. 3** High-fat diet alters the transcriptome of mouse liver tissue. (**A**) Heatmap showing the expression of DEGs in the HFD group and CON group. (**B**) Bar graph illustrating the number of DEGs. (**C-E**) GO enrichment analysis of DEGs, including (**C**) Biological Processes, (**D**) Cellular Components, and (**E**) Molecular Functions. (**F**) KEGG enrichment analysis of DEGs

with a protein band distribution consistent with the ideal scenario and no protein degradation observed (Figure S2A). Subsequently, we enzymatically digested the proteins and analyzed the resulting peptides using liquid chromatography-mass spectrometry (LC-MS). To ensure high-quality analysis results, we set a 1% False Discovery Rate (FDR) as the accuracy standard for data filtering at the level of spectra, peptides, and proteins (Figure S2B).

Proteins were identified only if they had at least one specific peptide. After completing the database search of the mass spectrometry raw data, we conducted quality control by assessing peptide length distribution, peptide count distribution, protein coverage distribution, and protein molecular weight distribution (Figure S2C-S2F). The evaluation results conformed to the general rules of mass spectrometric fragmentation and did not result in the loss of proteins within specific molecular weight ranges. Pearson's correlation coefficient (PCC), PCA, and Relative Standard Deviation (RSD) demonstrated excellent repeatability among our samples, with no outliers (Figure S2G-S2I). Box plots, distribution bar graphs, and density distribution curve graphs were used to illustrate the distribution and differences in protein intensity values among different samples (Figure S2J-S2L). The results showed good data distribution dispersion, intensity value distribution, and distribution of protein intensity values. In the proteomic analysis, differentially expressed proteins (DEPs) were analyzed with threshold criteria of $|FC| > 1.2$ and $p$-value $< 0.05$. Compared to the CON group, we identified 482 upregulated DEPs and 455 downregulated DEPs in the MASLD mouse model group, totaling 937 DEPs (Fig. 4A and B).

GO and KEGG enrichment analyses of the proteome are advantageous for revealing the biological functions and regulatory mechanisms of proteins. We selected the top 20 terms with the smallest $p$-values for analysis and subsequent display. At the BP level of GO enrichment, the enriched terms included important metabolic processes comprising the synthesis, breakdown, and transformation of molecules such as nucleotides, nucleosides, monocarboxylic acids, and ATP (Fig. 4C). At the CC level, the enriched terms included cytoplasm, organelles (such as mitochondria, peroxisomes, endoplasmic reticulum), cell membrane, and internal structures of organelles (such as matrix, lumen) (Fig. 4D). At the MF level, the enriched terms were related to various enzyme activities and binding properties (Fig. 4E). KEGG enrichment included various metabolic pathways such as steroid metabolism, lipid metabolism, amino acid metabolism, and sugar metabolism. Additionally, various types of biological defense and detoxification pathways were also enriched (Fig. 4F).

In summary, disruptions in both proteomic and transcriptomic profiles were observed during MASLD. However, the tendencies of dysregulation in GO/ KEGG pathways differ between the two omics layers. Hence, a combined analysis of the transcriptomic and proteomic data becomes imperative to gain a comprehensive understanding of the molecular mechanisms underlying MASLD.

### Similarities and differences in the proteomic and transcriptomic profiles of the MASLD mouse model

Transcriptomics and proteomics elucidate gene expression at the transcriptional and translational levels, respectively. Besides the straightforward one-to-one relationships between transcripts and proteins, there exist more complex regulatory interactions between the transcriptome and the proteome. Comparing the quantitative correlations between the two omics layers provides rapid insights into potential regulatory relationships between proteins and transcripts. We merged protein expression and mRNA expression by utilizing the correspondence between protein and transcript IDs. A scatter plot depicting the expression levels of transcripts and their corresponding proteins is shown in Fig. 5A. Through a combined analysis of protein and mRNA changes, we identified only 56 genes, 31 upregulated genes and 25 downregulated genes, showing a matching direction of change in both the proteome and transcriptome (Fig. 5B). Additionally, 848 genes exhibited no changes at the transcriptome level but showed significant alterations at the proteome level, suggesting the potential presence of post-transcriptional modifications (Fig. 5B).

Considering our earlier observation of significant abnormalities in m6A post-transcriptional modifications in MASLD, we focused our attention on the 442 genes upregulated at the protein level but unchanged at the transcript level and the 406 genes downregulated at the protein level but unchanged at the transcript level (Fig. 5B).

Based on our comparative analysis, we categorized proteins or transcripts according to different expression patterns, with each category corresponding to specific regulatory relationships (transcriptomic-proteomic: down-down, unchange-down, down-unchange, up-unchange, up-up, unchange-up). To gain further insights into the biological processes involved in proteins or transcripts exhibiting diverse regulatory relationships, we conducted KEGG and GO enrichment analyses using the Fisher exact test for each regulatory relationship. We selected GO functions/ KEGG pathways significantly enriched in at least one category ($p$-value $< 0.05$) and compared their enrichment levels among different protein categories using a heatmap. In the heatmap of the results, the x-axis represents different protein categories, the y-axis indicates GO functions/ KEGG pathways, and the color indicates the significance of enrichment (represented by $p$-value through $\log_{10}$ and Z-score transformation) (Fig. 5C and F).

The GO enrichment results revealed significant inconsistencies between the transcriptome and proteome across 56 BP categories (Fig. 5C). These processes included nucleotide metabolism, fatty acid metabolism, carboxylic acid metabolism, glucose metabolism,

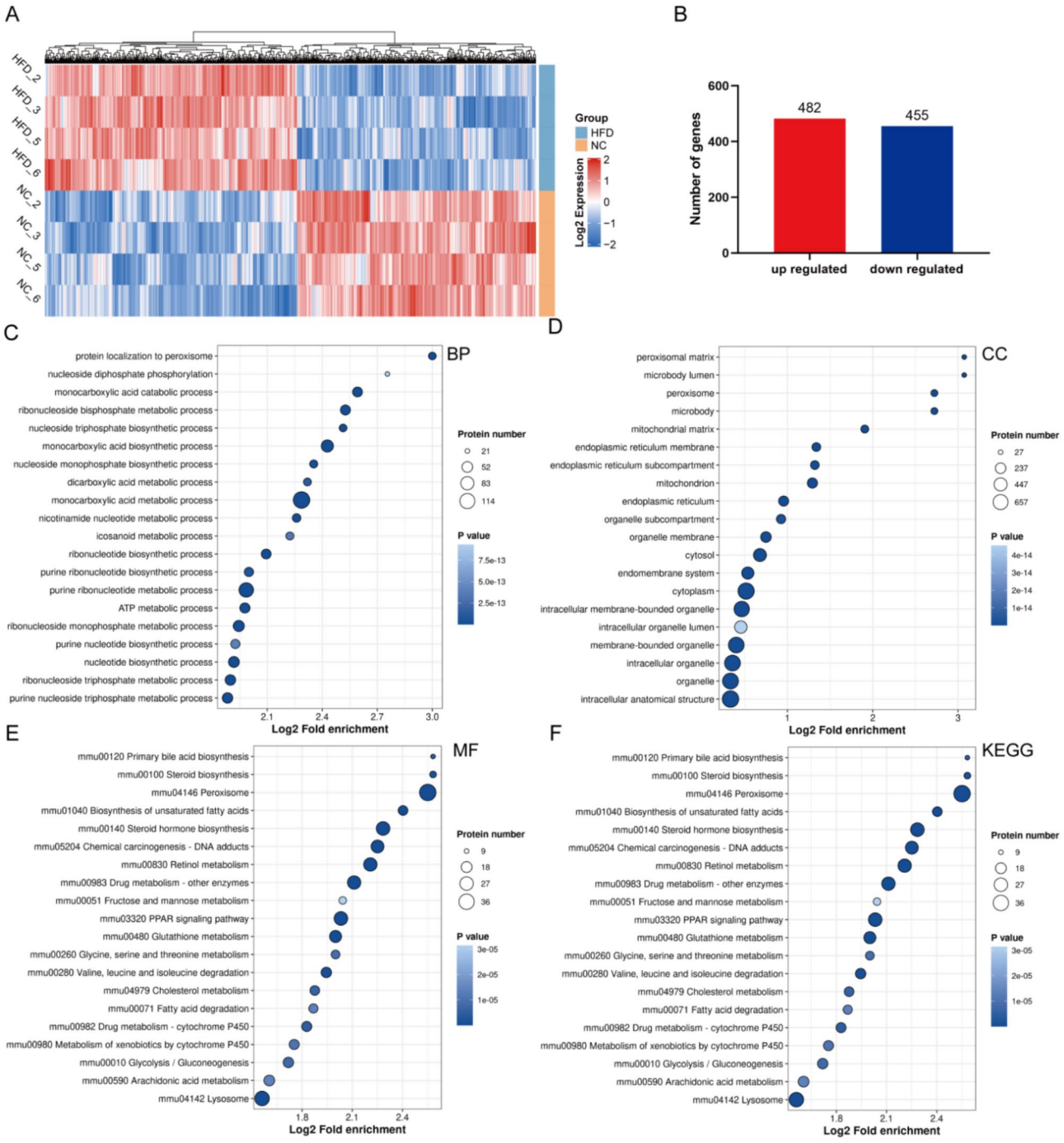


**Fig. 4** High-fat diet alters the proteome of mouse liver tissue. (**A**) Heatmap displaying the expression of DEPs in the HFD group and CON group. (**B**) Bar graph depicting the number of DEPs. (**C-E**) GO enrichment analysis of DEPs, including (**C**) Biological Processes, (**D**) Cellular Components, and (**E**) Molecular Functions. (**F**) KEGG enrichment analysis of DEPs

nucleoside and nucleotide biosynthesis, RNA processes, cellular responses, protein processes, and various other metabolic activities. Similarly, there were significant inconsistencies between the transcriptome and proteome across 36 CC categories (Fig. 5D). These included endoplasmic reticulum (ER) components, organelle components, lysosome and vacuole components, ribosome components, vesicle components, microbody and peroxisome components, mitochondria components, and lipid-related components. GO enrichment analysis also highlighted significant inconsistencies between the transcriptome and proteome across 59 MF components, primarily involving enzyme activity and binding activity (Fig. 5E). KEGG enrichment analysis revealed significant

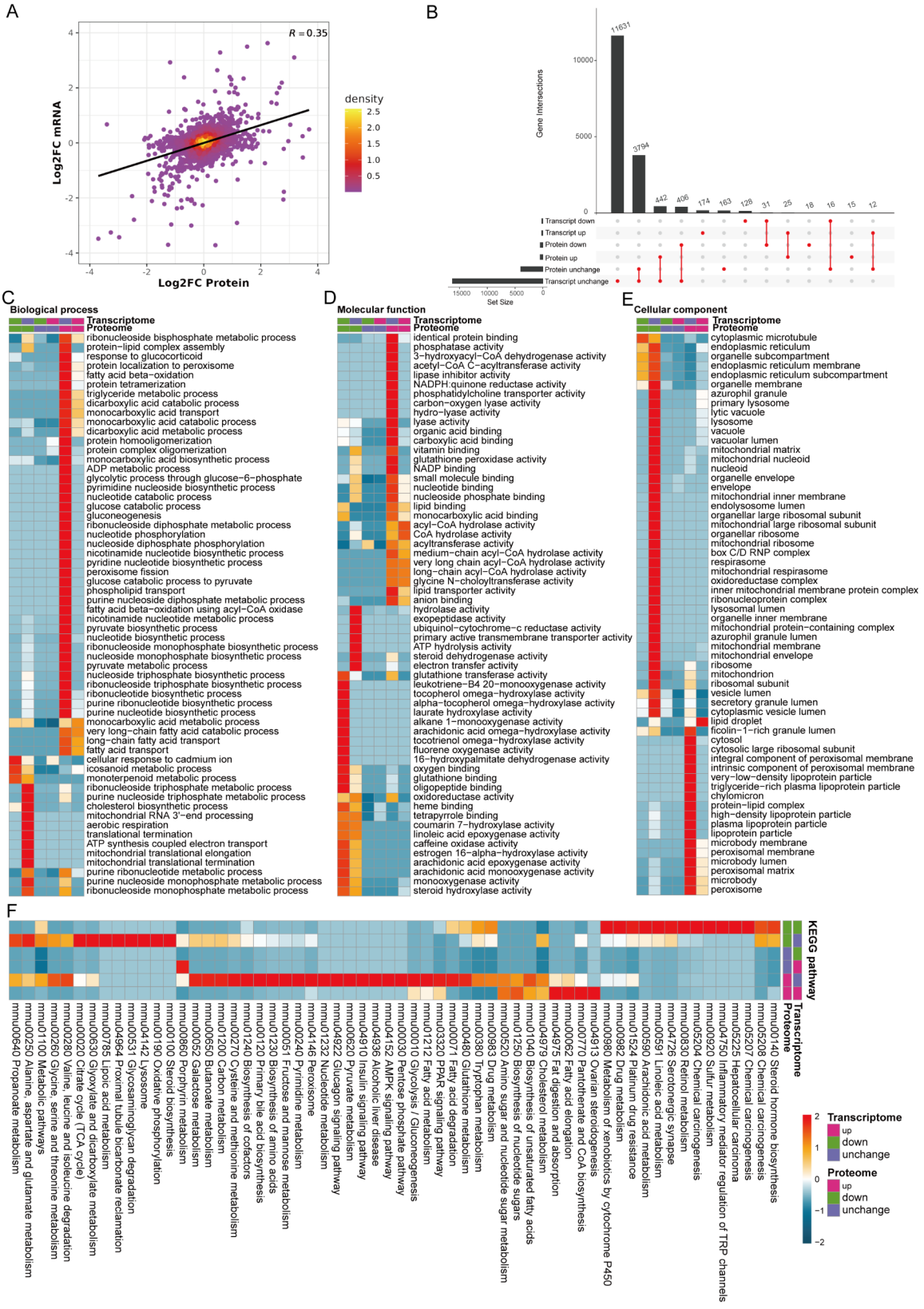


**Fig. 5** (See legend on next page.)

(See figure on previous page.)

**Fig. 5** Correlation analysis between transcriptome and proteome in the MASLD mouse model. (**A**) Scatter plot showing the expression levels of transcripts and their corresponding proteins. (**B**) Upset plot comparing the quantitative differences between the transcriptome and proteome. (**C-E**) Heatmaps illustrating the GO enrichment of proteins under different regulatory relationships between the transcriptome and proteome, including (**C**) Biological Processes, (**D**) Cellular Components, and (**E**) Molecular Functions. (**F**) Heatmap depicting the KEGG enrichment of proteins under different regulatory relationships between the transcriptome and proteome

inconsistencies between the transcriptome and proteome across 41 pathways (Fig. 5F). These pathways included lipid metabolism, nucleotide and nucleic acid metabolism, drug metabolism and detoxification, neurotransmitter and signaling pathways, carbohydrate metabolism, and amino acid metabolism.

#### METTL3 overexpression alters the hepatic proteome

To investigate the impact of METTL3 on liver cell function, we established a stable overexpression cell line in AML12 mouse liver cells using lentivirus ($p$-value = 0.0002) (Fig. 6A). We assessed the protein quality using Coomassie brilliant blue staining. The outcomes revealed distinct protein bands in all lanes, with the band distribution meeting the ideal criteria and no evidence of protein degradation (Figure S3A). Subsequently, we utilized LC-MS to enzymatically digest the proteins and analyze the resulting peptides. To ensure high-quality analysis outcomes, we employed a 1% FDR as the accuracy benchmark for data filtration across spectra, peptides, and proteins (Figure S3B). Protein identification necessitated the presence of at least one specific peptide. Upon completion of the database search for the mass spectrometry raw data, we conducted quality assessment by examining peptide length distribution, peptide count distribution, protein coverage distribution, and protein molecular weight distribution (Figure S3C-S3F). The evaluation results adhered to the typical principles of mass spectrometric fragmentation and did not result in protein loss within specific molecular weight ranges. PCC, PCA, and RSD indicated excellent reproducibility among our samples, with no outliers (Figure S3G-S3I). Box plots, distribution bar graphs, and density distribution curve graphs were employed to display the distribution and disparities in protein intensity values among various samples (Figure S3J-S3L). The findings showcased satisfactory data dispersion, intensity value distribution, and protein intensity value distribution. After stringent quality control procedures, we conducted a differential analysis of the protein mass spectrometry data between the Blank group and the METTL3 overexpression group (Fig. 6B). Using $|FC| < 1.2$ and $p$-value $< 0.05$ as threshold criteria for the analysis of Differentially Expressed Proteins (DEPs), we identified a total of 2397 differentially expressed proteins, including 1176 upregulated proteins and 1221 downregulated proteins (Fig. 6C and D).

Next, GO/ KEGG enrichment analyses were performed to reveal the biological processes influenced by METTL3 in the liver. The top 20 terms with the smallest $p$-values were selected for analysis and presentation. In the BP category, enriched terms included glycolysis and sugar metabolism, ketone metabolism, energy metabolism, and nucleotide biosynthesis and degradation processes (Fig. 6E). In the CC category, enriched terms included various cellular structures and functions, comprising components related to the cell membrane, cell nucleus, mitochondria, secretory vesicles and vacuoles, molecular machinery, and complexes, as well as components related to the cell skeleton and structure (Fig. 6F). These components have specific locations and functions within the cell, participating in physiological activities and biological processes such as signal transduction, energy metabolism, secretion, maintenance of the cell skeleton, and nuclear functions. In the MF category, enriched terms included terms related to oxidoreductase activity, membrane transport activity, ion channel and regulatory activity, hydrolase activity, and molecular binding activity (Fig. 6G). The KEGG enrichment analysis results were enriched for cellular processes such as sugar metabolism, energy metabolism, signal transduction, mineral balance, and some specific cellular processes (Fig. 6H).

#### Enrichment analysis of genes regulated by METTL3 in MASLD

To further explore the proteins regulated by METTL3 during MASLD, we conducted a combined analysis of highly expressed proteins in both the MASLD model group and the METTL3 overexpression group, revealing an overlap of 84 upregulated proteins (Fig. 7A). It is noteworthy that over 50% of the upregulated proteins primarily localize to the cytoplasm, with most of the remaining proteins exhibiting a nuclear localization, and a smaller fraction distributed among other cellular compartments (Fig. 7B).

Next, we performed GO enrichment analysis to elucidate the functions of METTL3-upregulated DEPs during MASLD. In the BP category, the upregulated DEGs were enriched for nucleotide biosynthetic processes, nucleotide metabolic processes, nucleotide phosphorylation, and glycolysis (Fig. 7C). At the CC level, the upregulated DEGs were enriched for terms including cytoplasm, lipid-related structures, microbodies, granules, and membranes (Fig. 7D). At the MF level, the upregulated DEGs were enriched for various functions and activities related to biology and biochemistry, including protein binding, catalytic activity, and molecular binding

(Fig. 7E). In addition, we employed KEGG enrichment to analyze the biological mechanisms enriched in METTL3-upregulated DEPs during MASLD. Among the top 20 enriched terms, many were related to glucose metabolism, lipid metabolism, and amino acid metabolism (Fig. 7F).

Through our combined analysis of the MASLD model group and the METTL3 overexpression group, we also identified 111 consistently downregulated DEPs (Fig. 8A). These downregulated DEPs primarily localize to mitochondria, followed by the cell membrane and extracellular space (Fig. 8B). GO and KEGG enrichment analyses provided an insight into the cellular localization and possible functions of these downregulated DEPs. At the BP level, the downregulated DEPs were mainly associated with energy conversion, membrane transport, nucleotide metabolism, as well as cholesterol and steroid metabolism (Fig. 8C). At the CC level, the downregulated DEPs were associated with mitochondria, organelles bounded by the inner membrane, vacuoles, and lysosomes (Fig. 8D). At the MF level, the downregulated DEPs were primarily associated with catalytic activity, transporter protein activity, and glycine N-acyltransferase activity (Fig. 8E). The results of KEGG enrichment analysis indicate significant enrichment in these downregulated DEPs for pathways related to organic acid metabolism, amino acid metabolism, steroid metabolism, as well as organelles and structural components (Fig. 8F).

#### Pathway enrichment of METTL3-induced m6a post-transcriptional modifications during MASLD

By comparing the transcriptome and proteome of an MASLD mouse model, we were able to identify several enriched pathways potentially related to post-transcriptional modifications. Additionally, through a comparison between the proteome of an MASLD mouse model and the proteome of liver cells overexpressing METTL3, we were able to identify the pathways regulated by METTL3 during MASLD. Our aim here is to integrate these two sets of bioinformatics annotations to identify the biological impacts of METTL3-mediated post-transcriptional modifications in MASLD.

First, we performed GO enrichment analysis of the integrated data. At the BP level, 24 co-enriched GO terms were identified. These terms encompass nicotinamide/ nicotinic acid metabolism, ketone body metabolism, nucleotide processes, carbohydrate metabolism, monocarboxylic acid metabolism, and cholesterol biosynthesis. At the CC level, we identified 27 co-enriched GO terms related to the cytoplasmic region, peroxisome, microbody, mitochondria, vacuole, lysosome, and other cellular organelles and membranes. At the MF level, 11 co-enriched GO terms were identified, and these mostly involved enzyme activities. Next, we performed KEGG pathway enrichment analysis of the integrated data. We were able to identify 25 co-enriched pathways covering fatty acid metabolism, amino acid metabolism, carbohydrate metabolism, steroid biosynthesis, and cellular organelles (Table S1).

#### Core node proteins regulated by METTL3 during MASLD

After conducting statistical analysis on the enriched pathways mentioned above, we identified a total of 158 DEPs. Next, the database identifiers or protein sequences of these DEPs were compared with the STRING protein-protein interaction network database. Based on a confidence score greater than 0.7 (high confidence), we extracted the interaction relationships among DEPs (Fig. 9A). On this basis, we selected proteins with five or more interactions as core node proteins in the protein-protein interaction network (PPI), resulting in a total of 11 core node proteins (Fig. 9B). These 11 hub genes were uploaded to the DSigDB database to predict potential small-molecule drugs for reversing MASLD. We selected the top ten small molecules based on $p$-values, including 7,8-Benzoflavone, pd 158,780, rosiglitazone, Vorinostat, acrylamide, 9001-31-4, fulvestrant PC3, ibuprofen, Plumbagin, and 2,6-dichloro-4-nitrophenol. These small molecule compounds have the potential to exert anti-MASLD effects by inhibiting the upregulation of hub genes (Figure S4). Among these hub genes, GAPDH, TPI1, and ENO1, which rank in the top three, have caught our attention. We validated the mRNA and protein levels of these genes in both animal and cellular models. The results closely matched our sequencing data. In the animal model, there was no significant difference in the mRNA levels of these three hub genes in the HFD group (Fig. 9C), while their protein levels were significantly enhanced (Fig. 9D and E). In cells with overexpression of METTL3, we observed similar results, with the exception of ENO1 (Fig. 9F and H).

## Discussion

While there has been significant research on m6A in the context of MASLD, few studies have investigated the role of METTL3 in the development and progression of MASLD through multi-omics integrated analysis. In this study, we employed multi-omics integrated analysis to conduct large-scale molecular profiling of animal and cell models of MASLD, with the aim of obtaining a comprehensive understanding of molecular-level processes such as disease mechanisms and cellular metabolism. In the animal model, a combined analysis of the transcriptome and proteome revealed that only 56 genes exhibited consistent changes at both protein and transcript levels. Hence, we infer the presence of extensive post-transcriptional and post-translational modifications in the MASLD mouse model. We shifted our focus towards the

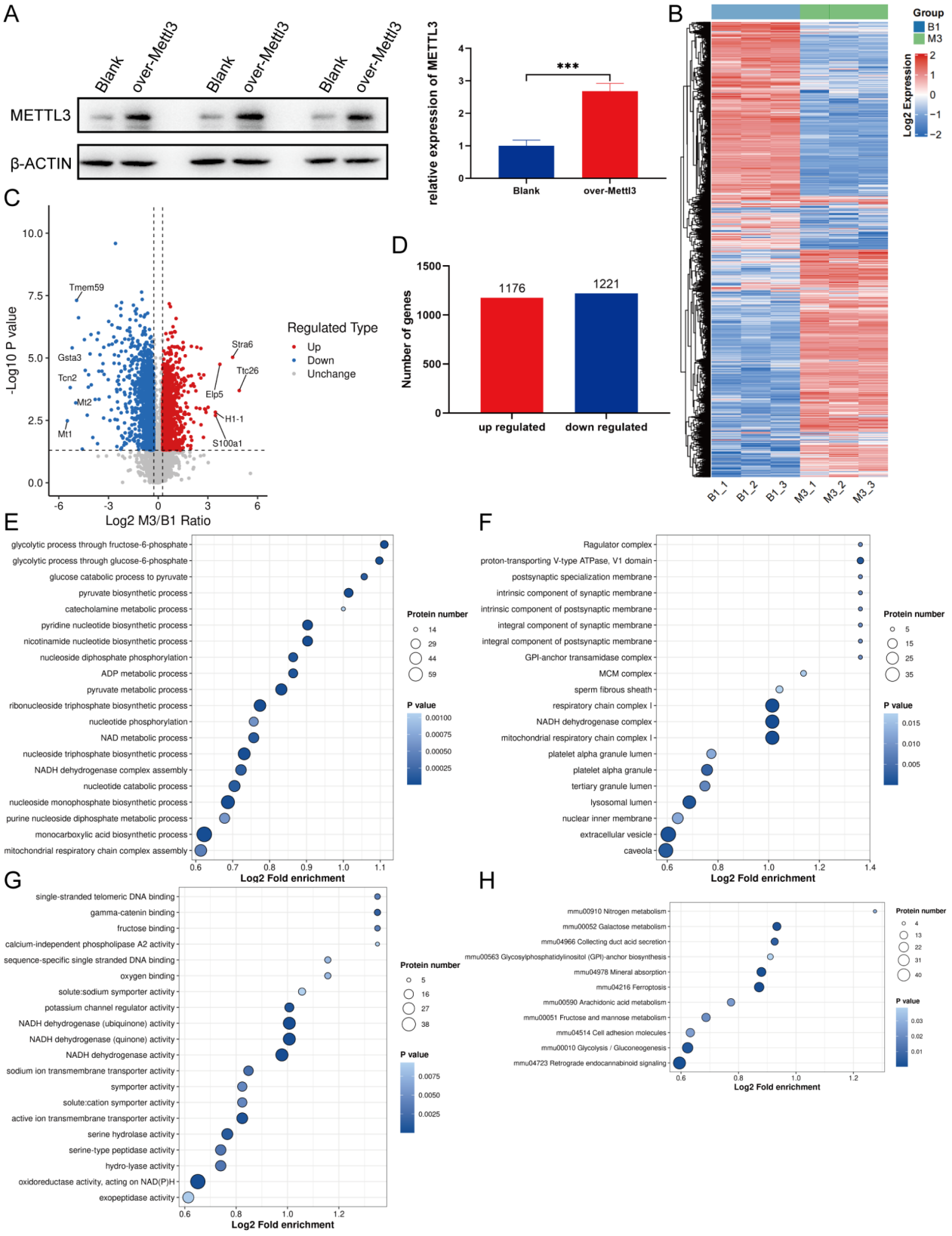


**Fig. 6** Overexpression of METTL3 alters the proteome in the liver. (**A**) Western blotting and quantitative analysis of METTL3 protein in AML12 cells transfected with overexpressing METTL3 lentivirus. (**B**) Heatmap displaying the expression of DEPs in the Blank group and over-METTL3 group. (**C**) Volcano plot illustrating the expression of DEPs. (**D**) Bar graph depicting the number of DEPs. (**E-G**) GO enrichment analysis of DEPs, including (**E**) Biological Processes, (**F**) Cellular Components, and (**G**) Molecular Functions. (**H**) KEGG enrichment analysis of DEPs. ($n = 3$, t-test, $^{*}p < 0.05$, $^{**}p < 0.01$, $^{***}p < 0.001$, $^{****}p < 0.0001$)

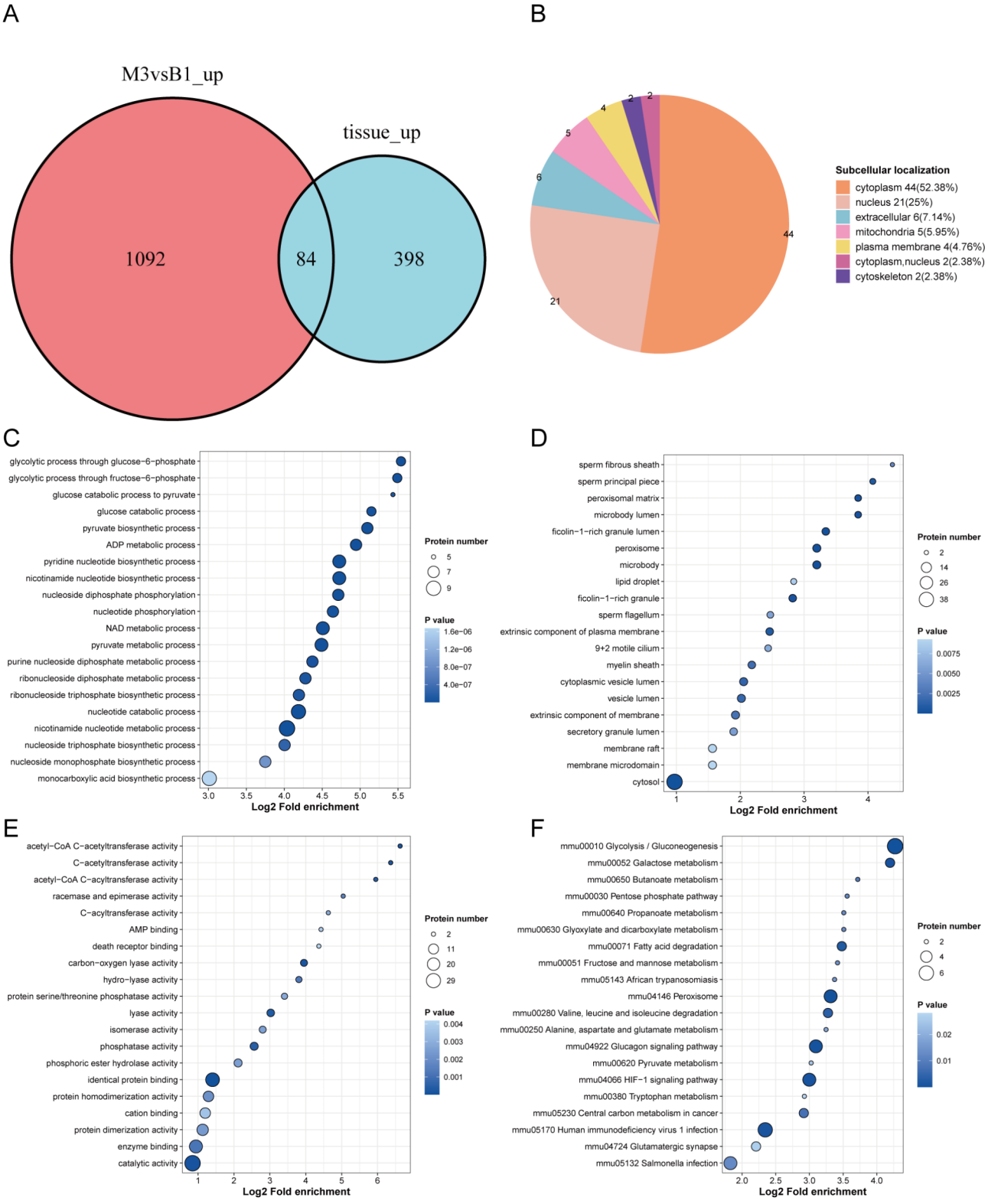


**Fig. 7** Integrative enrichment analysis of upregulated genes in the proteome of mouse and cell models with METTL3. (**A**) Venn diagram depicting the overlap between upregulated DEPs in the MASLD mouse model and the METTL3 overexpressing AML12 cell model. (**B**) Subcellular classification of commonly upregulated genes. (**C-E**) GO enrichment analysis of intersecting genes, including (**C**) Biological Processes, (**D**) Cellular Components, and (**E**) Molecular Functions. (H) KEGG enrichment analysis of commonly upregulated genes

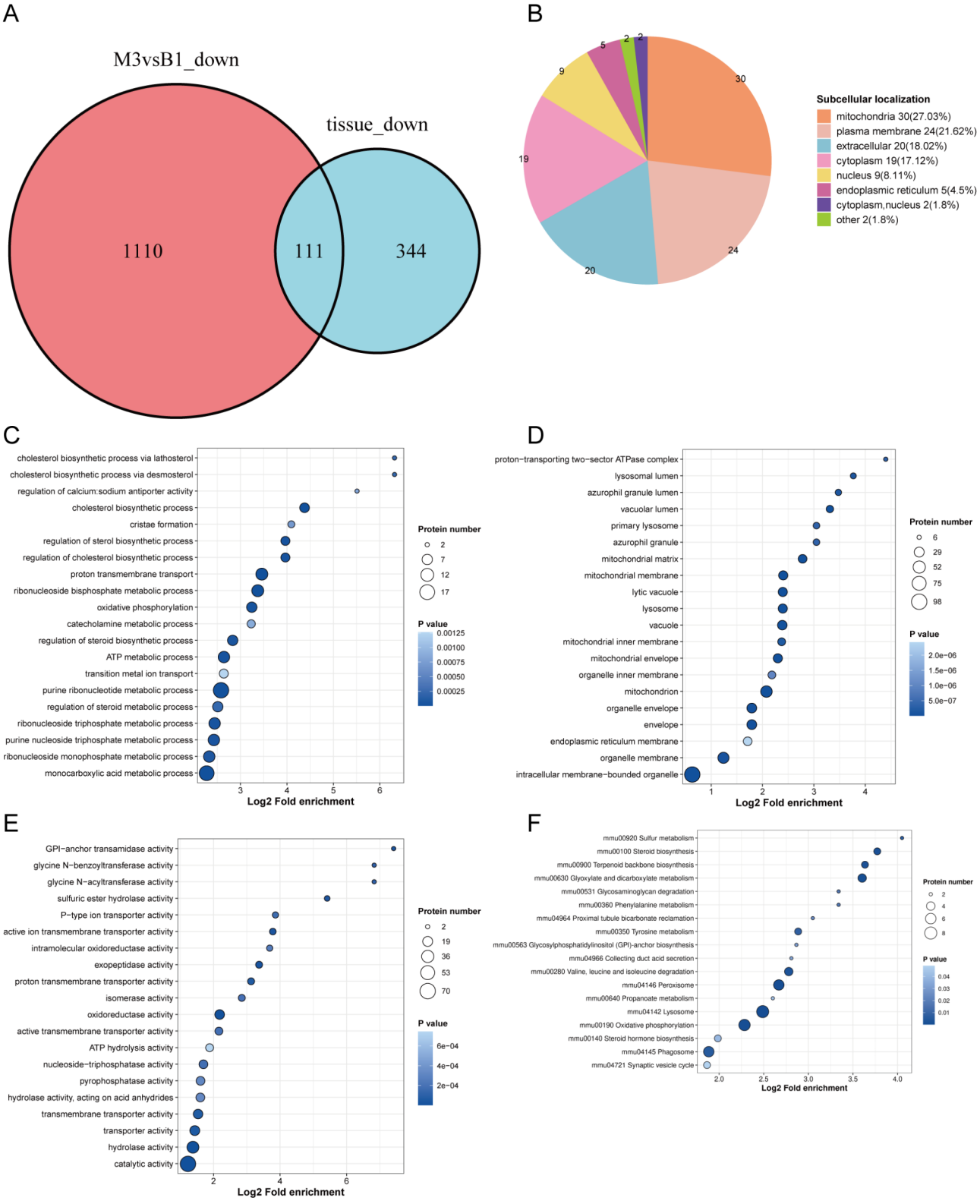


**Fig. 8** Integrative enrichment analysis of downregulated genes in the proteome of mouse and cell models with METTL3. (**A**) Venn diagram illustrating the overlap between downregulated DEPs in the MASLD mouse model and the METTL3 overexpressing AML12 cell model. (**B**) Subcellular classification of commonly downregulated genes. (**C-E**) GO enrichment analysis of intersecting genes, including (**C**) Biological Processes, (**D**) Cellular Components, and (**E**) Molecular Functions. (**H**) KEGG enrichment analysis of commonly downregulated genes

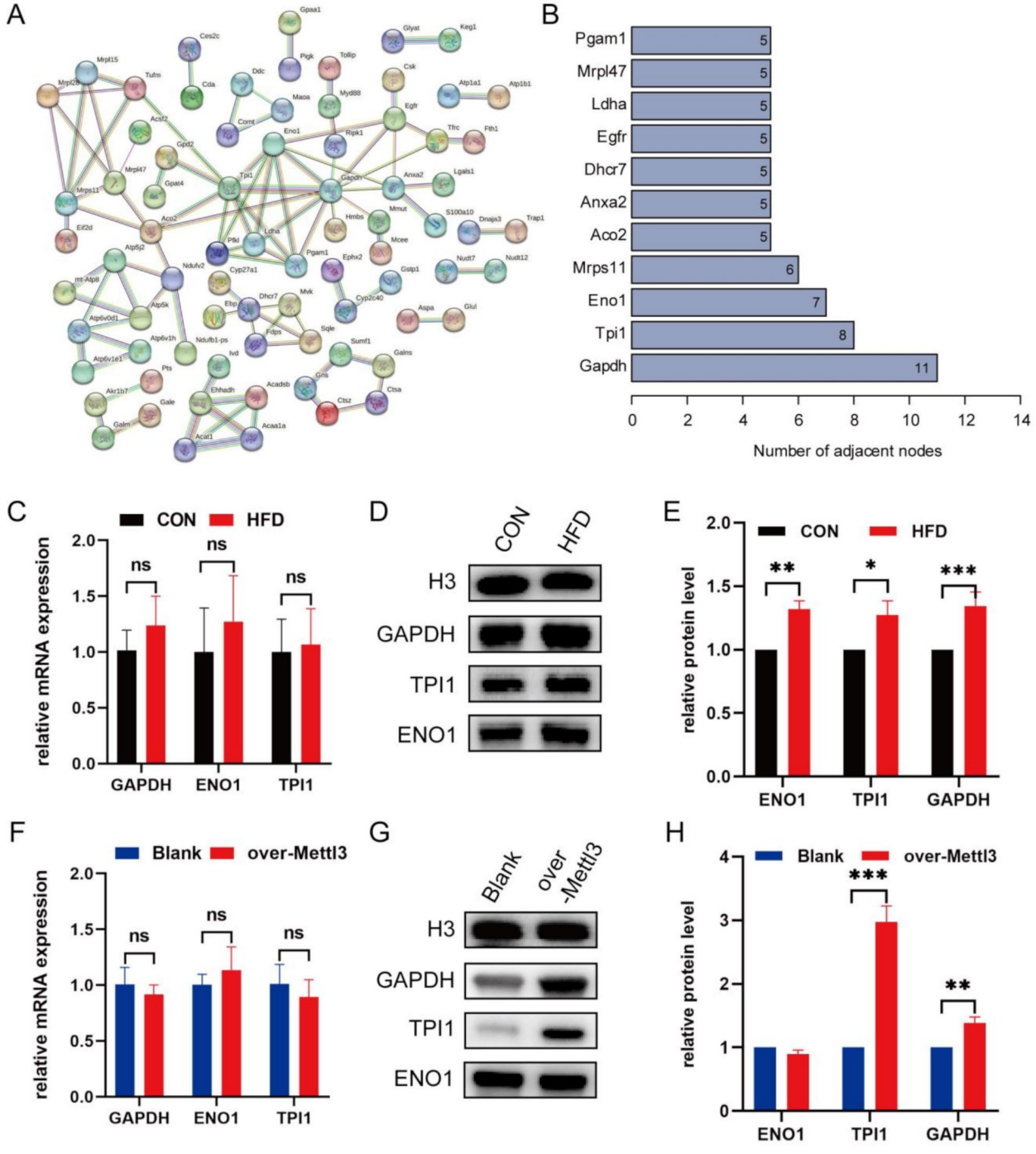


**Fig. 9** Core node proteins regulated by METTL3 in MASLD. (**A**) Protein-protein interaction network diagram of DEPs. (**B**) Statistical analysis of gene interactions. (**C**) qRT–PCR analysis of the mRNA expression levels of genes between control and HFD group. (**D and E**) Western blotting (**D**) and quantitative analysis (**E**) of the protein expression levels between control and HFD group. (**F**) qRT–PCR analysis of the mRNA expression levels of genes between blank and over-METTL3 group. (**G and H**) Western blotting (**G**) and quantitative analysis (**H**) of the protein expression levels between blank and over-METTL3 group

848 proteins that exhibited changes at the protein level despite no alterations at the transcriptome level. This approach allowed us to delve deeper into the molecular mechanisms underlying MASLD, and to identify potential therapeutic targets and prognostic markers.

We observed that upon METTL3 overexpression, the transcriptional levels of many genes remained unchanged. As a key regulator of the post-transcriptional m6A modification, METTL3 can modulate protein levels through various mechanisms, such as RNA modification, splicing, export, stability, and translation, without affecting transcription levels [37]. The limited impact of METTL3 overexpression on the proteome or transcriptome may result from a combination of factors, including the dynamic equilibrium of m6A modification, the complex regulation of mRNA stability and translation, and cellular compensation mechanisms [38]. Together, these factors enable METTL3 to regulate various biological processes in the cell without altering mRNA or protein levels.

Our subsequent analysis was grounded in pathway analysis rather than simple gene analysis because pathway analysis provides more comprehensive information, covering interactions between genes and signaling networks. Pathway analysis takes into account the collaborative interactions between genes, facilitating a better understanding of their overall functionality in biological processes. Compared to simple gene analysis, pathway analysis is more likely to reveal the overall changes and relationships associated with specific biological processes or disease states.

Using an approach involving integrative analysis of the transcriptome and proteome, we conducted GO and KEGG enrichment analyses for these proteins and selected the top 60 terms for each enrichment category for further analysis. We observed a substantial inconsistency between the enriched pathways in the transcriptome and proteome. In MASLD, the pathways identified are differentially regulated by post-transcriptional modifications, particularly m6A modification. The detection of high expression of METTL3 in the MASLD mouse model prompted our consideration of the role of METTL3-mediated m6A post-transcriptional modification in influencing the development of MASLD.

To elucidate the role of METTL3 in MASLD, we established a stable cell line overexpressing METTL3 in AML12 liver cells. Integrated proteomic analysis of mouse and cellular proteins revealed a total of 195 proteins that were consistently changed in both the MASLD mouse model group and the METTL3 overexpression group. These proteins are likely regulated by METTL3 during MASLD, and GO/ KEGG analyses identified associated terms indicative of METTL3 regulation. To confirm that the pathway alterations were specifically due to the impact of METTL3-induced m6A post-transcriptional modifications rather than other factors, we performed an intersection analysis of the enriched pathways identified in the two combined analyses. The resulting GO/ KEGG terms highlighted the major biological processes influenced by METTL3-induced m6A transcriptional modifications in MASLD, particularly the KEGG terms.

As shown in Table S1, the terms enriched in GO: BP primarily encompass nicotinamide/nicotinic acid metabolism, ketone body metabolism, nucleotide processes, carbohydrate metabolism, monocarboxylic acid metabolism, and cholesterol biosynthesis. Disruptions in nicotinamide/nicotinic acid metabolism can affect cellular energy metabolism and antioxidant capacity, thereby promoting the occurrence and progression of MASLD [39]. Abnormal ketone body metabolism may reflect a disruption in hepatic fatty acid metabolism, with excessive ketone body production and impaired utilization, potentially exacerbating the metabolic burden on the liver and leading to hepatocyte damage. Abnormal nucleotide processes can impair normal cellular functions and gene expression regulation, particularly affecting hepatocyte proliferation, apoptosis, and metabolic activity [40]. Disruption of carbohydrate metabolism leads to increased glucose uptake and utilization in the liver, promoting fat synthesis and accumulation, further aggravating hepatic steatosis. Additionally, carbohydrate metabolism disturbances may affect the liver's antioxidant defense system, increasing oxidative stress damage [41]. Abnormal monocarboxylic acid metabolism impacts cellular energy metabolism and signal transduction, promoting fat accumulation and inflammation in hepatocytes [42]. Alterations in cholesterol biosynthesis could result in excessive cholesterol accumulation in the liver, forming cholesterol crystals that trigger inflammatory responses and hepatocyte damage, contributing to the progression of MASLD [43]. In GO: CC, the enriched GO terms are related to the cytoplasmic region, peroxisomes, microbodies, mitochondria, vacuoles, lysosomes, and other cellular organelles and membranes. The cytoplasm is the primary site for various metabolic activities within the cell, including fatty acid synthesis and ketone body formation, both of which are relevant to MASLD. Abnormalities in the cytoplasmic region could affect the transport of metabolic substances and enzyme activity, leading to metabolic disorders that promote the onset and progression of MASLD. Dysfunction of peroxisomes disrupts fatty acid metabolism, resulting in an excess of peroxides and free radicals, inducing oxidative stress damage and worsening hepatocyte injury [44]. Abnormalities in microbody function may impair the liver's ability to clear metabolic toxins, exacerbating liver damage and advancing MASLD. Mitochondrial dysfunction can lead to impaired

fatty acid oxidation, generating excessive reactive oxygen species (ROS), causing oxidative stress, damaging cellular functions, and promoting hepatocyte apoptosis and inflammation [45]. Vacuoles may play a role in lipid storage and transport, and dysfunction here may lead to abnormal lipid accumulation within the cell, worsening hepatic steatosis. Lysosomal dysfunction can cause impaired degradation of lipid metabolites, leading to the formation of lipid peroxidation products, which trigger inflammation and hepatocyte damage [44]. In GO: MF, most of the enriched terms are associated with enzyme activity, participating in fatty acid synthesis, oxidation, and cholesterol metabolism. Abnormal enzyme activity could be an early signal of NAFLD onset.

In MASLD, the upregulated KEGG pathways influenced by METTL3-induced m6A modifications included five terms related to carbohydrate metabolism: mmu00010, Glycolysis / Gluconeogenesis; mmu00052, Galactose metabolism; mmu00051, Fructose and mannose metabolism; mmu00030, Pentose phosphate pathway; and mmu00620, Pyruvate metabolism. These pathways interact with each other to ensure cellular energy and metabolic balance. Additionally, they contribute to enhanced lipid accumulation through a mechanism involving Enhanced glycolysis. Here, glycolysis, the process of converting glucose into pyruvate, is intensified. Pyruvate is a crucial precursor for fatty acid biosynthesis, and these pyruvates can be further converted into fatty acids or triglycerides. Increased pyruvate metabolism is known to augment the rate of fatty acid synthesis [46]. High-fructose-fed mice exhibit increased METTL3 transcript expression and elevated m6A levels, and these adaptations are associated with changes in the expression of genes related to glucose metabolism [30]. Augmented metabolism of galactose and fructose produces metabolites that can enter glycolysis or the pentose phosphate pathway, increasing glucose supply and energy synthesis, thereby promoting lipid synthesis [46]. After activation of the pentose phosphate pathway, NADPH generated by the pentose phosphate pathway can be utilized for fatty acid synthesis. Thus, NADPH provides reducing equivalents for fatty acid synthase (FASN), using acetyl-CoA as a primer and malonyl-CoA as a two-carbon donor to synthesize fatty acids [47, 48].

In total, the enriched GO and KEGG pathways collectively encompassed 158 DEPs. Through PPI network analysis, we identified 11 genes that interacted with other genes in more than five instances. Subsequently, we utilized the DSigDB database to predict potential small molecule drugs for these 11 genes. This step is crucial to reducing research and development costs during subsequent MASLD drug development, to expanding the range of drug development choices, and to facilitating a more comprehensive understanding of the correlation between drugs and gene expression. Furthermore, it facilitates a deeper exploration of the mechanisms of action of these drugs, thereby providing a solid theoretical foundation for subsequent research endeavors.

Among these hub genes, GAPDH, ENO1 and TPI1 caught our attention. However, we found that while ENO1 expression increased in the animal model, there was no significant change in ENO1 expression in METTL3-overexpressing cells. This discrepancy may be due to the complexity of animal models, where high-fat feeding not only increases METTL3 expression but also affects other signaling pathways. These pathways may involve signaling between different cell types and inter-organ communication. In contrast, cell models represent a more controlled environment, where METTL3 overexpression only influences intracellular processes. The increased expression of ENO1 in the MASLD mouse model, but not in the cell model, suggests that the regulation may not be solely mediated by METTL3. Therefore, these two genes can be considered as key hub genes influenced by METTL3 during MASLD (Fig. 10). These genes occupy central positions in the expression network, directly or indirectly interacting with many other genes, thus playing crucial roles in regulating biological processes.

Conventionally, GAPDH (Glyceraldehyde-3-phosphate dehydrogenase) is considered highly conserved, and GAPDH is commonly used as an internal control in studies of gene expression regulation. However, evidence supporting the regulation of GAPDH expression itself under certain conditions is accumulating, especially because of its association with MASLD and type 2 diabetes [49–51]. GAPDH is a key rate-limiting enzyme in the glycolytic pathway [52], catalyzing the reaction of glyceraldehyde-3-phosphate to 1,3-bisphosphoglycerate, generating NADH that can participate in processes such as oxidative phosphorylation [52]. GAPDH, as a central step in glycolysis, serves as a convergence point for monosaccharides entering either the glycolytic pathway or the pentose phosphate pathway. According to Shestov et al., when upstream substrates of GAPDH are abundant, glycolysis is primarily controlled by GAPDH. Conversely, when substrates upstream of GAPDH are limited, glycolysis is primarily regulated by other upstream rate-limiting enzymes [53]. This theory concerning the changing role of GAPDH may provide new insights into MASLD research.

GAPDH is also known to stimulate terminal glycolysis during the late interphase. Its activity promotes the activities of PGK1 and PKM2, generating ATP, while LDH-5 regenerates $NAD^+$ for GAPDH function. Activation of PKM2 releases PEP from TPI-induced cleavage. Thus, DHAP synthesis is activated, maintaining the synthesis of glycerol phosphate required for triglyceride

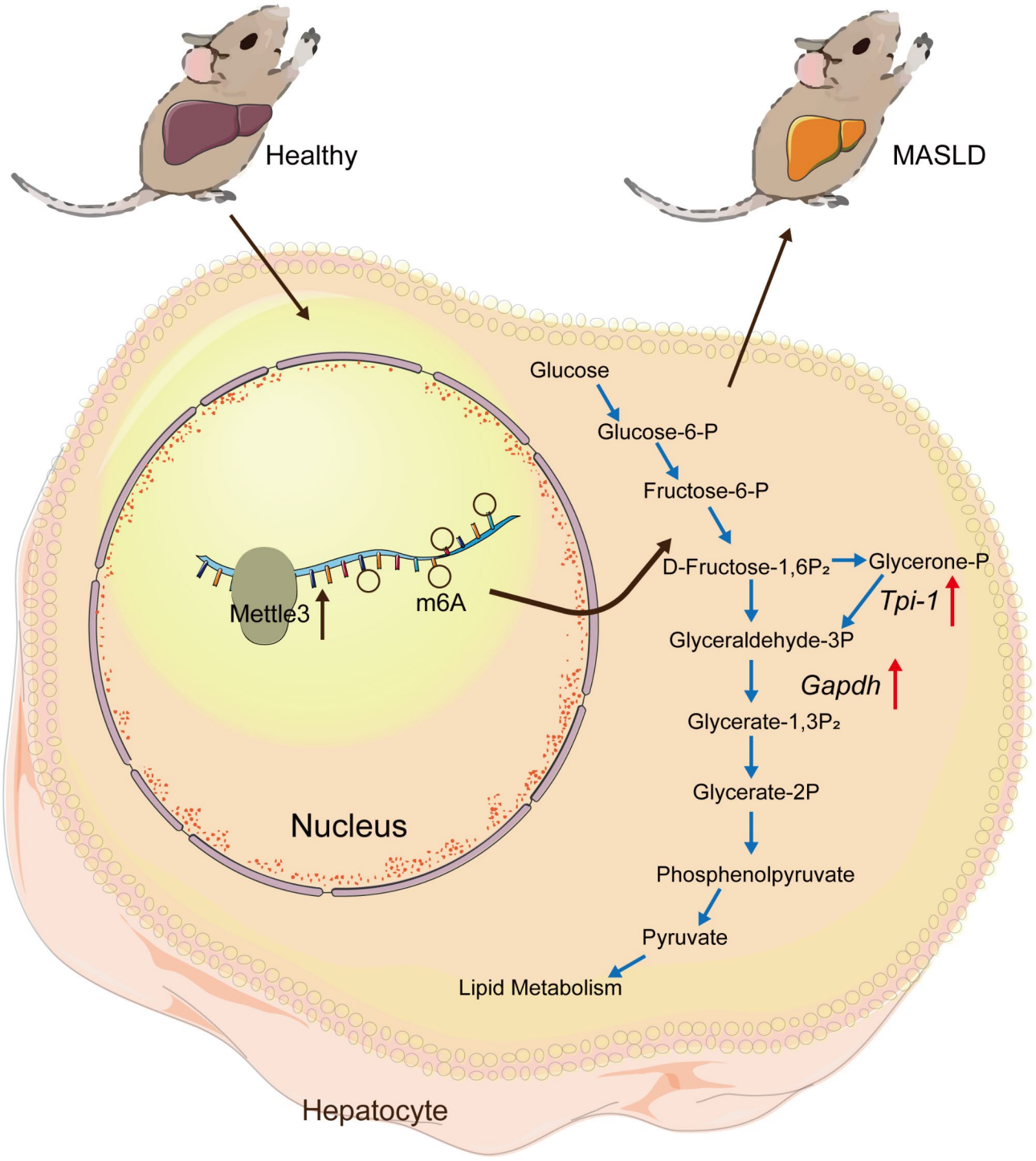


**Fig. 10** Proposed mechanism diagram

formation [54]. TPI1 (Triosephosphate isomerase 1) is encoded by a single gene located on the short arm of chromosome 12 (12q13). This stable dimer exhibits high conservation across numerous organisms. In the glycolytic pathway, TPI enzyme catalyzes the interconversion of dihydroxyacetone phosphate (DHAP) and glyceraldehyde-3-phosphate (G3P), serving as a key catalytic enzyme in both glycolysis and gluconeogenesis [55, 56]. TPI1 facilitates the conversion of phosphoenolpyruvate in glycolysis, which is crucial for lipid metabolism processes such as fatty acid synthesis, beta-oxidation, and phospholipid biosynthesis. Glyceraldehyde-3-phosphate

is also a key molecule in the pentose phosphate pathway. Because of the convoluted metabolic interconnections within cells, the many different metabolic processes can influence each other. Therefore, TPI1 may impact multiple intracellular energy metabolism processes such as glycolysis, gluconeogenesis, lipid metabolism, and the pentose phosphate pathway [57].

## Conclusions

During MASLD, the hepatic glycolytic process may be influenced by hepatic fat deposition and cellular dysfunction, leading to modulation of the expression levels and activities of GAPDH and TPI1. These modifications reflect changes in liver metabolism, energy demand, and energy supply regulation. Regulation of the glycolytic pathway and these two hub genes by the key m6A post-transcriptional modifier METTL3 likely contributes to the pathogenesis of MASLD. This insight aids in understanding the potential of METTL3 as a disease regulatory factor in MASLD, paving the way for novel therapeutic approaches in future MASLD research.

## Supplementary Information

The online version contains supplementary material available at https://doi.org/10.1186/s12864-025-11377-4.

Supplementary Material 1

Supplementary Material 2

**Acknowledgements**
We want to thank MogoEdit (https://www.mogoedit.com) for its English editing during the preparation of this manuscript.

**Author contributions**
These authors contributed equally: S.W, Z.X. S.W., Z.X. and J.W. conceived and designed the experiments; S.W. and Z.X. performed most experiments and data analysis; Z.W. and X.Y. contributed to data interpretation and prepared consumables; S.W. and Z.X. wrote the manuscript; J.W. revised the manuscript. All authors contributed to editorial changes in the manuscript. All authors read and approved the final manuscript.

**Funding**
The study was funded by the Beijing Natural Science Foundation, grant number 7244288; Capital Institute of Pediatrics basic special key funding project, grant number JCYJ-2025-11.

**Data availability**
The datasets presented in this study can be found in online repositories. The names of the repository/repositories and accession number(s) can be found below: http://www.proteomexchange.org/,PXD047819; http://www.proteomexchange.org/,PXD050565; https://www.ncbi.nlm.nih.gov/sra/,PRJNA1052390.

## Declarations

**Ethics approval and informed consent**
The study was conducted according to the guidelines of the Declaration of Helsinki, and approved by The Ethics Committee on Animal Care and Use of the Capital Institute of Pediatrics (SHERLL2021032).

**Consent for publication**
Not applicable.

**Competing interests**
The authors declare no competing interests.

Received: 11 September 2024 / Accepted: 18 February 2025
Published online: 24 February 2025

**References**

1. Ayonrinde OT. Historical narrative from fatty liver in the nineteenth century to contemporary NAFLD - reconciling the present with the past. JHEP Rep. 2021;3:100261. https://doi.org/10.1016/j.jhepr.2021.100261
2. Rinella ME, Lazarus JV, Ratziu V, Francque SM, Sanyal AJ, Kanwal F, et al. A multisociety Delphi consensus statement on new fatty liver disease nomenclature. Hepatology. 2023;78:1966–86. https://doi.org/10.1097/HEP.0000000000000520
3. Song SJ, Lai JC, Wong GL, Wong VW, Yip TC. Can we use old NAFLD data under the new MASLD definition? J Hepatol. 2024;80:e54–6. https://doi.org/10.1016/j.jhep.2023.07.021
4. Rinella ME, Neuschwander-Tetri BA, Siddiqui MS, Abdelmalek MF, Caldwell S, Barb D, et al. AASLD practice guidance on the clinical assessment and management of nonalcoholic fatty liver disease. Hepatology. 2023;771797–835. https://doi.org/10.1097/HEP.0000000000000323
5. Sarwar R, Pierce N, Koppe S. Obesity and nonalcoholic fatty liver disease: current perspectives. Diabetes Metab Syndr Obes. 2018;11:533–42. https://doi.org/10.2147/DMSO.S146339
6. Sutti S, Albano E. Adaptive immunity: an emerging player in the progression of NAFLD. Nat Rev Gastroenterol Hepatol. 2020;17:81–92. https://doi.org/10.1038/s41575-019-0210-2
7. Zhai M, Liu Z, Long J, Zhou Q, Yang L, Zhou Q, et al. The incidence trends of liver cirrhosis caused by nonalcoholic steatohepatitis via the GBD study 2017. Sci Rep. 2021;11:5195. https://doi.org/10.1038/s41598-021-84577-z
8. Goyal NP, Schwimmer JB. The progression and natural history of pediatric nonalcoholic fatty liver disease. Clin Liver Dis. 2016;20:325–38. https://doi.org/10.1016/j.cld.2015.10.003
9. Mitsinikos T, Mrowczynski-Hernandez P, Kohli R. Pediatric nonalcoholic fatty liver disease. Pediatr Clin North Am. 2021;68:1309–20. https://doi.org/10.1016/j.pcl.2021.07.013
10. Jobira B, Frank DN, Silveira LJ, Pyle L, Kelsey MM, Garcia-Reyes Y, et al. Hepatic steatosis relates to gastrointestinal microbiota changes in obese girls with polycystic ovary syndrome. PLoS ONE. 2021;16e0245219. https://doi.org/10.1371/journal.pone.0245219
11. Wang C, Pai AK, Putra J. Paediatric non-alcoholic fatty liver disease: an approach to pathological evaluation. J Clin Pathol. 2022;75:443–51. https://doi.org/10.1136/jclinpath-2022-208246
12. Vos MB, Van Natta ML, Blondet NM, Dasarathy S, Fishbein M, Hertel P et al. Randomized placebo-controlled trial of losartan for pediatric NAFLD. Hepatology. 2022;76:429–44. https://doi.org/10.1002/hep.32403
13. Younes R, Bugianesi E. Should we undertake surveillance for HCC in patients with NAFLD? J Hepatol. 2018;68:326–34. https://doi.org/10.1016/j.jhep.2017.10.006
14. O'Hara J, Finnegan A, Dhillon H, Ruiz-Casas L, Pedra G, Franks B, et al. Cost of non-alcoholic steatohepatitis in Europe and the USA: the GAIN study. JHEP Rep. 2020;2:100142. https://doi.org/10.1016/j.jhepr.2020.100142
15. Zhou B, Liu C, Xu L, Yuan Y, Zhao J, Zhao W, et al. N(6) -methyladenosine reader protein YT521-B homology domain-containing 2 suppresses liver steatosis by regulation of mRNA stability of lipogenic genes. Hepatology. 2021;73:91–103. https://doi.org/10.1002/hep.31220
16. Li Z, Qi J, Liu H, Tang Y, Liu J, Sun C. Abnormal m6A modification in non-alcoholic fatty liver disease. Zhong Nan Da Xue Xue Bao Yi Xue Ban. 2021:46785–92. https://doi.org/10.11817/j.issn.1672-7347.2021.210264
17. Luo Y, Zhang Z, Xiang L, Zhou B, Wang X, Lin Y, et al. Analysis of N6-methyladenosine methylation modification in fructose-induced non-alcoholic fatty liver disease. Front Endocrinol (Lausanne). 2021;12:780617. https://doi.org/10.3389/fendo.2021.780617
18. Luo Z, Zhang Z, Tai L, Zhang L, Sun Z, Zhou L. Comprehensive analysis of differences of N(6)-methyladenosine RNA methylomes between high-fat-fed and normal mouse livers. Epigenomics. 2019;11:1267–82. https://doi.org/10.2217/epi-2019-0009
19. Cheng W, Li M, Zhang L, Zhou C, Yu S, Peng X, et al. New roles of N6-methyladenosine methylation system regulating the occurrence of non-alcoholic

fatty liver disease with N6-methyladenosine-modified MYC. Front Pharmacol. 2022;13:973116. https://doi.org/10.3389/fphar.2022.973116
20. Harrahill NJ, Hadden MK. Small molecules that regulate the N(6)-methyladenosine RNA modification as potential anti-cancer agents. Eur J Med Chem. 2024;274:116526. https://doi.org/10.1016/j.ejmech.2024.116526
21. Zhang Y, Chen W, Zheng X, Guo Y, Cao J, Zhang Y, et al. Regulatory role and mechanism of m(6)A RNA modification in human metabolic diseases. Mol Ther Oncolytics. 2021;22:52–63. https://doi.org/10.1016/j.omto.2021.05.003
22. Liu J, Yue Y, Han D, Wang X, Fu Y, Zhang L, et al. A METTL3-METTL14 complex mediates mammalian nuclear RNA N6-adenosine methylation. Nat Chem Biol. 2014;10:93–5. https://doi.org/10.1038/nchembio.1432
23. Knuckles P, Lence T, Haussmann IU, Jacob D, Kreim N, Carl SH, et al. Zc3h13/Flacc is required for adenosine methylation by bridging the mRNA-binding factor Rbm15/Spenito to the m(6)A machinery component Wtap/Fl(2)d. Genes Dev. 2018;32:415–29. https://doi.org/10.1101/gad.309146.117
24. Bawankar P, Lence T, Paolantoni C, Haussmann IU, Kazlauskiene M, Jacob D, et al. Hakai is required for stabilization of core components of the m(6)A mRNA methylation machinery. Nat Commun. 2021;12:3778. https://doi.org/10.1038/s41467-021-23892-5
25. Wang P, Doxtader KA, Nam Y. Structural basis for cooperative function of METTL3 and Mettl14 methyltransferases. Mol Cell. 2016;63:306–17. https://doi.org/10.1016/j.molcel.2016.05.041
26. Peng Z, Gong Y, Wang X, He W, Wu L, Zhang L, et al. METTL3-m(6)A-Rubicon axis inhibits autophagy in nonalcoholic fatty liver disease. Mol Ther. 2022;30:932–46. https://doi.org/10.1016/j.ymthe.2021.09.016
27. Qin Y, Li B, Arumugam S, Lu Q, Mankash SM, Li J, et al. m(6)A mRNA methylation-directed myeloid cell activation controls progression of NAFLD and obesity. Cell Rep. 2021;37:109968. https://doi.org/10.1016/j.celrep.2021.109968
28. Xie W, Ma LL, Xu YQ, Wang BH, Li SM. METTL3 inhibits hepatic insulin sensitivity via N6-methyladenosine modification of Fasn mRNA and promoting fatty acid metabolism. Biochem Biophys Res Commun. 2019;518:120–6. https://doi.org/10.1016/j.bbrc.2019.08.018
29. Zhong X, Yu J, Frazier K, Weng X, Li Y, Cham CM, et al. Circadian clock regulation of hepatic lipid metabolism by modulation of m(6)A mRNA methylation. Cell Rep. 2018;25:1816–28. https://doi.org/10.1016/j.celrep.2018.10.068
30. Li Y, Zhang Q, Cui G, Zhao F, Tian X, Sun BF, et al. m(6)A regulates liver metabolic disorders and hepatogenous diabetes. Genomics Proteom Bioinf. 2020;18:371–83. https://doi.org/10.1016/j.gpb.2020.06.003
31. Ferguson D, Finck BN. Emerging therapeutic approaches for the treatment of NAFLD and type 2 diabetes mellitus. Nat Rev Endocrinol. 2021;17:484–95. https://doi.org/10.1038/s41574-021-00507-z
32. De Masi A, Li X, Lee D, Jeon J, Wang Q, Baek S, et al. Cyclo(His-Pro): A further step in the management of steatohepatitis. JHEP Rep. 2023;5:100815. https://doi.org/10.1016/j.jhepr.2023.100815
33. Wang S, Zhang W, Wang Z, Liu Z, Yi X, Wu J. METTL3-m6A-YTHDF1 axis promotion of mitochondrial dysfunction in metabolic dysfunction-associated steatotic liver disease. Cell Signal. 2024;121:111303. https://doi.org/10.1016/j.cellsig.2024.111303
34. Wang S, Wang Z, Liu Z, Wu J. Prognostic value of four immune-related genes in lower-grade gliomas: a biomarker discovery study. Front Genet. 2024;15:1403587. https://doi.org/10.3389/fgene.2024.1403587
35. Lu Z, Qian P, Chang J, He X, Zhang H, Wu J, et al. Multi-omics analysis explores the effect of chronic exercise on liver metabolic reprogramming in mice. Front Cell Dev Biol. 2023;11:1199902. https://doi.org/10.3389/fcell.2023.1199902
36. Qian P, Ma F, Zhang W, Cao D, Li L, Liu Z, et al. Chronic exercise remodels the lysine acetylome in the mouse hippocampus. Front Mol Neurosci. 2022;15:1023482. https://doi.org/10.3389/fnmol.2022.1023482
37. Barbieri I, Kouzarides T. Role of RNA modifications in cancer. Nat Rev Cancer. 2020;20:303–22. https://doi.org/10.1038/s41568-020-0253-2
38. Yang Y, Hsu PJ, Chen YS, Yang YG. Dynamic transcriptomic m(6)A decoration: writers, erasers, readers and functions in RNA metabolism. Cell Res. 2018;28:616–24. https://doi.org/10.1038/s41422-018-0040-8
39. Zhou J, Han J. Association of niacin intake and metabolic dysfunction-associated steatotic liver disease: findings from National health and nutrition examination survey. BMC Public Health. 2024;24:2742. https://doi.org/10.1186/s12889-024-20161-0
40. Peng L, Xiang S, Wang T, Yang M, Duan Y, Ma X, et al. The hepatic clock synergizes with HIF-1alpha to regulate nucleotide availability during liver damage repair. Nat Metab. 2025. https://doi.org/10.1038/s42255-024-01184-8
41. Santamarina AB, Sertorio MN, Mennitti LV, Souza EA, Souza DV, Ribeiro DA, et al. Hepatic effects of low-carbohydrate diet associated with different lipid sources: insights into oxidative stress, cytotoxicity, and epigenetic markers in a mouse model of obesity. J Nutr. 2024;154:1517–31. https://doi.org/10.1016/j.tjnut.2024.03.007
42. Weiss JM, Palmieri EM, Gonzalez-Cotto M, Bettencourt IA, Megill EL, Snyder NW, et al. Itaconic acid underpins hepatocyte lipid metabolism in non-alcoholic fatty liver disease in male mice. Nat Metab. 2023;5:981–95. https://doi.org/10.1038/s42255-023-00801-2
43. Duan Y, Gong K, Xu S, Zhang F, Meng X, Han J. Regulation of cholesterol homeostasis in health and diseases: from mechanisms to targeted therapeutics. Signal Transduct Target Ther. 2022;7:265. https://doi.org/10.1038/s41392-022-01125-5
44. Lai Y, Liu CW, Yang Y, Hsiao YC, Ru H, Lu K. High-coverage metabolomics uncovers microbiota-driven biochemical landscape of interorgan transport and gut-brain communication in mice. Nat Commun. 2021;12:6000. https://doi.org/10.1038/s41467-021-26209-8
45. Mu C, Wang S, Wang Z, Tan J, Yin H, Wang Y, et al. Mechanisms and therapeutic targets of mitochondria in the progression of metabolic dysfunction-associated steatotic liver disease. Ann Hepatol. 2024;101774. https://doi.org/10.1016/j.aohep.2024.101774
46. Sanders FW, Griffin JL. De Novo lipogenesis in the liver in health and disease: more than just a shunting yard for glucose. Biol Rev Camb Philos Soc. 2016:91452–68. https://doi.org/10.1111/brv.12178
47. Lupu R, Menendez JA. Pharmacological inhibitors of fatty acid synthase (FASN)--catalyzed endogenous fatty acid biogenesis: a new family of anti-cancer agents? Curr Pharm Biotechnol. 2006;7:483–93. https://doi.org/10.2174/138920106779116928
48. Buckley D, Duke G, Heuer TS, O'Farrell M, Wagman AS, McCulloch W, et al. Fatty acid synthase - modern tumor cell biology insights into a classical oncology target. Pharmacol Ther. 2017;177:23–31. https://doi.org/10.1016/j.pharmthera.2017.02.021
49. Comajoan P, Gubern C, Huguet G, Serena J, Kadar E, Castellanos M. Evaluation of common housekeeping proteins under ischemic conditions and/or rt-PA treatment in bEnd.3 cells. J Proteom. 2018:18410–5. https://doi.org/10.1016/j.jprot.2018.06.011
50. Goasdoue K, Awabdy D, Bjorkman ST, Miller S. Standard loading controls are not reliable for Western blot quantification across brain development or in pathological conditions. Electrophoresis. 2016;37:630–4. https://doi.org/10.1002/elps.201500385
51. Haythorne E, Lloyd M, Walsby-Tickle J, Tarasov AI, Sandbrink J, Portillo I, et al. Altered glycolysis triggers impaired mitochondrial metabolism and mTORC1 activation in diabetic beta-cells. Nat Commun. 2022;13:6754. https://doi.org/10.1038/s41467-022-34095-x
52. Semenyuk P, Barinova K, Muronetz V. Glycation of alpha-synuclein amplifies the binding with glyceraldehyde-3-phosphate dehydrogenase. Int J Biol Macromol. 2019;127:278–85. https://doi.org/10.1016/j.ijbiomac.2019.01.064
53. Shestov AA, Liu X, Ser Z, Cluntun AA, Hung YP, Huang L, et al. Quantitative determinants of aerobic glycolysis identify flux through the enzyme GAPDH as a limiting step. Elife. 2014;3. https://doi.org/10.7554/eLife.03342
54. Gruning NM, Du D, Keller MA, Luisi BF, Ralser M. Inhibition of triosephosphate isomerase by phosphoenolpyruvate in the feedback-regulation of glycolysis. Open Biol. 2014;4:130232. https://doi.org/10.1098/rsob.130232
55. Oliver C, Timson DJ. In silico prediction of the effects of mutations in the human triose phosphate isomerase gene: towards a predictive framework for TPI deficiency. Eur J Med Genet. 2017;60:289–98. https://doi.org/10.1016/j.ejmg.2017.03.008
56. Jiang H, Ma N, Shang Y, Zhou W, Chen T, Guan D, et al. Triosephosphate isomerase 1 suppresses growth, migration and invasion of hepatocellular carcinoma cells. Biochem Biophys Res Commun. 2017;482:1048–53. https://doi.org/10.1016/j.bbrc.2016.11.156
57. Pekel G, Ari F. Therapeutic targeting of cancer metabolism with triosephosphate isomerase. Chem Biodivers. 2020;17e2000012. https://doi.org/10.1002/cbdv.202000012

## Publisher's note